Development/Plasticity/Repair

Large-Scale Somatotopic Refinement via Functional Synapse Elimination in the Sensory Thalamus of Developing Mice

Yuichi Takeuchi,[1,2,3] Hidetsugu Asano,[4,5] Yoko Katayama,[1] Yoshihiro Muragaki,[4,6] Keiji Imoto,[2,3] and Mariko Miyata[1,7]

[1]Department of Physiology, School of Medicine, Tokyo Women's Medical University, Tokyo 162-8666, Japan, [2]Department of Physiological Sciences, School of Life Science, The Graduate University for Advanced Studies (SOKENDAI), Okazaki 444-8787, Japan, [3]Department of Information Physiology, National Institute for Physiological Sciences, Okazaki 444-8787, Japan, [4]Faculty of Advanced Techno-Surgery, Institute of Advanced Biomedical Engineering and Science, Graduate School of Medicine, Tokyo Women's Medical University, Tokyo 162-8666, Japan, [5]Research and Development Division, Pioneer Corporation, Kanagawa 212-0031, Japan, [6]Department of Neurosurgery, School of Medicine, Tokyo Women's Medical University, Tokyo 162-8666, Japan, and [7]Precursory Research for Embryonic Science and Technology, Japan Science and Technology Agency, Saitama 332-0012, Japan

Functional synapse elimination and strengthening are crucial developmental processes in the formation of precise neuronal circuits in the somatosensory system, but the underlying alterations in topographical organization are not yet fully understood. To address this issue, we generated transgenic mice in which afferent fibers originating from the whisker-related brain region, called the maxillary principal trigeminal nucleus (PrV2), were selectively visualized with genetically expressed fluorescent protein. We found that functional synapse elimination drove and established large-scale somatotopic refinement even after the thalamic barreloid architecture was formed. Before functional synapse elimination, the whisker sensory thalamus was innervated by afferent fibers not only from the PrV2, but also from the brainstem nuclei representing other body parts. Most notably, only afferent fibers from PrV2 onto a whisker sensory thalamic neuron selectively survived and were strengthened, whereas other afferent fibers were preferentially eliminated via their functional synapse elimination. This large-scale somatotopic refinement was at least partially dependent on somatosensory experience. These novel results uncovered a previously unrecognized role of developmental synapse elimination in the large-scale, instead of the fine-scale, somatotopic refinement even after the initial segregation of the barreloid map.

Introduction

Functional synapse elimination and synapse strengthening are essential for the formation of precise neuronal circuits during development, including the refinement of topographical information (Purves and Lichtman, 1980; Wong and Lichtman, 2003; Kano and Hashimoto, 2009). However, the actual relationship between functional synapse elimination and refinement of topographical information remains unclear because most synapse elimination studies have been conducted without identifying which types of fibers survive and which do not.

The whisker sensory thalamus of mice (the ventral posteromedial nucleus; VPM) is a favorable system for this study in that sensory afferents (lemniscal fibers) can be characterized according to their somatotopic information because the VPM has a visible somatosensory map called the barreloid architecture (Sugitani et al., 1990; Land et al., 1995; Haidarliu and Ahissar, 2001). The mouse barreloid is established by postnatal day 5 (P5) and contains a complete representation of the whiskers (Van der Loos, 1976; Belford and Killackey, 1979; Yamakado, 1985). Whisker-mediated sensory information is conveyed by the maxillary branch of the trigeminal nerves (V2) and is then synaptically transmitted to the ventrolateral subregion of the principal trigeminal nucleus (Pr5). From the V2 region of Pr5 (PrV2), lemniscal fibers convey information to the contralateral VPM. After barreloid formation, redundant lemniscal fibers on each thalamic neuron are functionally eliminated, so that only one lemniscal fiber per neuron typically survives and is strengthened from P7–P16 (Arsenault and Zhang, 2006). Therefore, to date, the functional elimination of lemniscal fibers, instead of large-scale somatosensory segregation, has been thought to be the critical step in the refinement of neuronal connections onto a single thalamic neuron.

To understand how somatotopic information is refined during functional synapse elimination, we genetically labeled lemniscal fibers originating from PrV2 using a Krox20-Cre knock-in mouse line and a Cre-dependent tdTomato reporter line (Ai14; Voiculescu et al., 2000; Madisen et al., 2010). Krox20, a transcription factor in the developing hindbrain, has a specific expression pattern with rhombomere 3, which corresponds to PrV2, includ-

Received Sept. 10, 2013; revised Nov. 9, 2013; accepted Dec. 5, 2013.

Author contributions: M.M. designed research; Y.T. and Y.K. performed research; H.A., Y.M., and K.I. contributed unpublished reagents/analytic tools; Y.T. analyzed data; Y.T. and M.M. wrote the paper.

This work was supported by the Japan Scientific and Technology Agency Precursory Research for Embryonic Science and Technology Program (Grants-in-Aid for Scientific Research (18500316, 20021029, 22800063, 23500400, 25870757, 09J00032), the Science Research Promotion Fund of The Promotion and Mutual Aid Corporation for Private School of Japan, Narishige Neuroscience Research Foundation, Terumo Life Science Foundation, the Naito Science and Engineering Foundation, and the Takeda Science Foundation. We thank E. Naraba and M. Hatakenaka for technical assistance; F.M. Rijli and T. Iwasato for the gift of Krox20-Cre mice; M. Watanabe and M. Yamasaki for technical suggestions; and Y. Honda for support with the Neurolucida system.

The authors declare no competing financial interests.

Correspondence should be addressed to Mariko Miyata, Department of Physiology, School of Medicine, Tokyo Women's Medical University, 8-1 Kawada-cho, Shinjuku-ku, Tokyo 162-8666, Japan. E-mail: mmiyata@research.twmu.ac.jp.

DOI:10.1523/JNEUROSCI.3865-13.2014

 0270-6474/14/341258-13$15.00/0

ing the barrelette region (Seitanidou et al., 1997; Oury et al., 2006). Therefore, by crossing Krox20-Cre and Ai14 lines, PrV2-origin lemniscal fibers can be labeled with tdTomato fluorescence throughout their axons from a very early embryonic stage. Using these mice, we sequentially analyzed structural and functional changes of developing lemniscal synapses to establish whether any correlation exists between the refinement of somatotopic information and functional synapse elimination. We found that the large-scale refinement of somatotopic information progresses and is completed through functional synapse elimination, even after the somatotopic information is somewhat segregated by barreloid formation. Furthermore, we uncovered a direct interaction between functional synapse elimination and somatotopic refinement by demonstrating that both are consistently disrupted by whisker deprivation.

Materials and Methods

Animals

All experiments were approved by the Animal Care and Use Committee of the Tokyo Women's Medical University and performed according to institutional guidelines. Krox20-Cre mice (Voiculescu et al., 2000) were backcrossed onto C57BL/6 for more than three generations before use. Cre-dependent tdTomato reporter mice (*ROSA26tm14*(*CAG-tdTomato*), Ai14) were introduced from The Jackson Laboratory (Madisen et al., 2010). To visualize lemniscal fibers, male Krox20-Cre heterozygotes and female Ai14 homozygotes were crossed and Cre-positive pups (Krox20-Ai14 mice) were used. Wild-type C57BL/6 mice were purchased from SLC. Mice were provided with a commercial diet and water *ad libitum* with controlled temperature, humidity, and lighting (12 h light/dark cycle). Both sexes of P0–P39 mice were used. Numbers of mice used were 85 Krox20-Ai14 and 99 wild-type.

Genotyping

Krox20-Cre mice were genotyped by a standard PCR procedure with Cre primers (Iwasato et al., 2004). Krox20-Ai14 pups were genotyped by PCR and/or detecting tdTomato signals in vibrissal follicles expressed from late pregnancy (Voiculescu et al., 2000). Results of both typing methods were always consistent.

Whisker deprivation

All mystacial vibrissae on the left side of the snout were deprived every other day from P12–P13 to the recording or perfusion day. Under a dissecting microscope, vibrissae of isoflurane-anesthetized mice were carefully plucked out using fine tweezers by applying slow, steady tension to the base of the vibrissa until the vibrissa slipped out of the follicle (Arsenault and Zhang, 2006; Wang and Zhang, 2008; Takeuchi et al., 2012).

Electrophysiology

Preparation of acute thalamic slices. Mice were anesthetized with isoflurane (Abbott) and decapitated. Parasagittal 250- to 300-μm-thick thalamic slices (Arsenault and Zhang, 2006; Takeuchi et al., 2012) were prepared using a microslicer (VT1200S; Leica Microsystems) in an ice-cold cutting solution containing the following (in mM): 234 sucrose, 2.5 KCl, 1.25 NaH_2PO_4, 10 $MgCl_2$, 0.5 $CaCl_2$, 25 $NaHCO_3$, 0.5 *myo*-inositol, and 11 glucose equilibrated with 95% O_2-5% CO_2. Slices were recovered in artificial CSF (ACSF) containing the following (in mM): 125 NaCl, 2.5 KCl, 1.25 NaH_2PO_4, 1 $MgSO_4$, 2 $CaCl_2$, 26 $NaHCO_3$, and 20 glucose equilibrated with 95% O_2-5% CO_2 at 32°C for 30 min and then kept at room temperature. A slice in a recording chamber was perfused by 30–32°C ACSF at a rate of 2.5–3.0 ml min^{-1}. During recordings, 10 μM (−)-bicuculline methochloride, 1 μM CGP55845, and 1 μM strychnine were included in the superfusate.

Whole-cell voltage-clamp recordings of lemniscal EPSCs

The tip resistance of the patch pipette was 2–5 MΩ when filled with an intracellular solution containing the following (in mM): 120 $CsMeSO_3$, 10 HEPES, 1 EGTA, 2 $MgCl_2$, 0.1 $CaCl_2$, 20 NaCl, 5 QX-314, 2 ATP-Na_2, 0.5 GTP-Na, and 0.5% biocytin, pH 7.3, 290–300 mOsm. Liquid junction potential was not compensated. Recordings were made from neurons in the VPM under infrared-differential interference contrast view of an upright microscope (BX51WI; Olympus). On slices of Krox20-Ai14 mice, recordings were made under guidance of tdTomato-labeled lemniscal fibers using a Nipkow-disk confocal unit (CSU-X1; Yokogawa Electric) with a cooled CCD camera (iXon DV898; Andor Technology; see Fig. 7) or a fluorescent cube with a mercury lamp (Olympus). Recordings were performed using a MultiClamp700A amplifier (MDS) and an ITC-18 AD/DA board (HEKA Elektronik) with Igor Pro software (Wavemetrics). Signals were filtered at 3 kHz and digitized at 50 kHz. The series resistance was compensated. If series resistance varied by >20% or increased >20 MΩ, the data were discarded. Data analysis was performed using Igor Pro.

Lemniscal fiber responses

A concentric bipolar electrode was placed on the medial lemniscal fiber bundle and electrical square pluses were then delivered at 0.1 Hz (100 μs duration, typically 10–400 μA; Takeuchi et al., 2012). We ensured that recorded synaptic currents were from lemniscal fibers, not from corticothalamic fibers, by following established criteria (Takeuchi et al., 2012): Depression of EPSCs in response to routinely applied paired-pulse stimuli with a 50 ms interstimulus interval (Castro-Alamancos, 2002; Miyata and Imoto, 2006); All-or-none or stepwise increments with the distinct threshold(s) in response to increasing stimulus intensity (Castro-Alamancos, 2002; Arsenault and Zhang, 2006; Miyata and Imoto, 2006) and faster rise time (typically <1 ms; Miyata and Imoto, 2006). Lemniscal EPSCs displayed the paired-pulse depression throughout development (P0–P39) and measured depression values were not different between ages (data not shown; Arsenault and Zhang (2006)).

Evaluation of lemniscal fiber innervations

To determine the number of lemniscal inputs for each thalamic neuron, lemniscal EPSCs were evoked at −70 mV and +40 mV (AMPAR- and NMDAR-medicated EPSCs, respectively) from the same neuron over a wide range of stimulus intensities as described previously (Takeuchi et al., 2012). Briefly, EPSC steps were first searched using 50 μA increments (Fig. 1*A*). After that, small increments were used in the order of 25, 10, 5, and 1 μA near each transition point to ensure that it was indeed a single step with a stable response. The step number of NMDAR-mediated EPSC was considered to be the number of lemniscal fiber inputs because NMDAR-mediated EPSCs have more reliable and discrete steps than AMPAR-mediated ones and lemniscal AMPAR-mediated synaptic responses during P0–P13 often showed silent synapses (data not shown). The fiber fraction (the amount of EPSC by minimally stimulated single fiber as a fraction of the maximal EPSC for each neuron; Hooks and Chen, 2006) and the contribution ratio (the largest single fiber-mediated EPSC as a fraction of the maximal EPSC for each neuron) were also calculated by NMDAR-mediated EPSCs.

Evoked miniature EPSCs at lemniscal synapses

Slices were perfused with modified ACSF, substituting 4 mM Sr^{2+} ions for Ca^{2+} ions in the presence of 100 μM $_{DL}$-APV at −90 mV (Takeuchi et al., 2012). Test stimulations were delivered at 0.1 Hz and at a sufficient intensity to reliably activate all lemniscal fibers innervating the recorded neuron. The time window for analysis was 100–500 ms after each stimulus. Miniature EPSCs were detected and analyzed by a semiautomated Igor Pro procedure.

Visualization of thalamic neurons

After electrophysiological recordings, slices were fixed with 4% paraformaldehyde in 0.1 M PB overnight. Biocytin-filled thalamic neurons were then visualized by a standard ABC-DAB reaction with cytochrome oxidase (CO) or methyl green counter staining or Alexa Fluor 633-conjugated streptavidin with DAPI (Takeuchi et al., 2012). Projection images of thalamic neurons were drawn using a camera lucida. For quantitative analyses, thalamic neurons were three-dimensionally reconstructed and analyzed using a computer-assisted microscope system (Eclipse E800; Nikon) with a 40× PlanApo objective lens (40×/0.95;

Nikon) and Neurolucida/Neurolucida Explore software (MBF Bioscience; Honda et al., 2012).

Histology

Perfusion/sectioning. Mice were deeply anesthetized with pentobarbital intraperitoneally and transcardially perfused with ice-cold saline followed by 4% paraformaldehyde and 0.2% picric acid in 0.1 M PB (pH 7.2–7.3). After removal, brains were postfixed overnight, infiltrated with sucrose gradient, blocked, and frozen on dry ice. VPM sections (20 μm thickness) at a plane perpendicular to the longest axis of most of barreloid units (barreloid plane; Haidarliu and Ahissar, 2001) were made using a freezing microtome unless otherwise noted. Sections were collected in antifreeze solution, rinsed in 0.1 M PBS, and then subjected to staining described in the sections below. All stainings were performed at room temperature unless otherwise noted.

CO staining

Sections were incubated with 0.05% 3,3′-diaminobenzidine, 0.03% cytochrome C, and 4% sucrose in 0.1 M PB at 37°C overnight. After washing with PBS, sections were mounted on gelatin-coated glass slides, dehydrated, cleared, and coverslipped. Images were acquired at 4020 × 3072 resolution using an upright microscope with a 10×/0.40 objective lens and a CCD camera (DP70; Olympus).

Acetylcholine esterase staining

Sections were stained as described by Watson and Paxinos (2010). The sections were then mounted, dehydrated, cleared, and coverslipped. Images were acquired as CO sections.

VGluT2 immunohistochemistry

All incubations were followed by washing with PBS containing 0.3% Triton X-100 (PBS-X). Sections were incubated successively with 10% normal goat serum (NGS) in PBS-X for 30 min, 1 μg/ml guinea pig anti-VGluT2 polyclonal antibody (VGluT2-GP-Af240 or 670; Frontier Science; Miyazaki et al., 2003) in PBS-X containing 1% NGS and 0.02% sodium azide (PBS-XG) overnight, and 1 μg/ml Alexa Fluor 633-conjugated goat anti-guinea pig IgG (A-21105; Invitrogen) for 2 h. Sections were then mounted and coverslipped with 50% glycerol and 2.5% triethylene diamine in PBS. If needed, sections were counterstained by a fluorescent Nissl staining solution (N-21479 or N-21480; Invitrogen).

tdTomato immunohistochemistry

After quenching by 0.3% H_2O_2 for 30 min, 20-μm-thick cryostat sections were successively incubated with 1:5000 rabbit anti-DsRed antibody (#632496; Clontech Laboratories) in PBS-XCG (0.12% λ-carrageenan, 1% NGS, and 0.02% sodium azide in PBS-X) overnight, 1.5 μg/ml biotinylated second antibody in PBS-XCG (BA-100; Vector Laboratories) for 2 h, and 1:100 ABC (Vector Laboratories) for 1 h. Sections were then subjected to BT-GO reaction for signal amplification for 30 min (Kuramoto et al., 2009) and incubated with ABC for 1 h again. The signals were localized with a standard peroxidase/DAB reaction with nickel enhancement. After stopping the reaction with 0.2% sodium azide, sections were mounted, counterstained with neutral red, dehydrated, cleared, and coverslipped.

PSD95 or GluA3 and VGluT2 double immunohistochemistry

Mice were fixed and the brains were removed. After an overnight postfix, 50-μm-thick thalamic frontal-plane sections were made with a vibrating blade microtome (VT1000S; Leica Microsystems). Sections were first subjected to PBS-X (0.1% Triton X-100 in PBS) and pepsin solution (1 mg/ml in 0.2N HCl/PBS-X) at 37°C for 30 min and 3 min, respectively (Fukaya and Watanabe, 2000). Sections were successively incubated with 10% NGS in PBS-X for 30 min, a mixture of first antibodies in PBS-XG (rabbit anti-PSD95: PSD95-Rb-Af628 or rabbit anti-GluA3: GluR3C-Rb-Af1090 and guinea pig anti-VGluT2: VGluT2-GP-Af670, 1 μg/ml for each; Frontier Science; Miyazaki et al., 2003) overnight, and a mixture of second antibodies in PBS-XG (Pacific blue-conjugated goat anti-rabbit IgG: P-10994 and Alexa Fluor 633-conjugated goat anti-guinea pig IgG: A-21105; Invitrogen) for 2 h. Sections were then mounted and coverslipped.

Retrograde labeling of ascending projection neurons in the brainstem

Mice at P11–PP28 were anesthetized by 1–3% isoflurane and placed on a stereotaxic frame. A small volume (0.25–0.40 μl) of 0.5% cholera toxin B subunit (CTB) biotin conjugate in 50 mM PBS (C9972; Sigma) was unilaterally injected into the whisker sensory thalamus (coordinates in mm: 1.35–1.60 posterior and 1.70–1.85 lateral to the bregma, 2.90–3.20 below the dura, depending on the age) through a micro needle syringe (NF35BV and NANOFIL; WPI) by continuous pressure from a microsyringe pump (53311; Stoelting). After 2 d of survival, mice were transcardially perfused and transverse brainstem sections (20 μm thickness) were prepared using a freezing microtome. For fluorescent localization, sections were incubated successively with 10% normal rabbit serum (NRS) in PBS-X containing 0.12% λ-carrageenan, 1% NRS, and 0.02% sodium azide (PBS-XCR) for 30 min, 1:10,000 goat anti-CTB antibody in PBS-XCR (703; List Biological Laboratories; Nakamura et al., 2005) overnight, 3.75 μg/ml biotinylated rabbit anti-goat IgG in PBS-XCR (BA-5000; Vector Laboratories) for 2 h, and 2.5 μg/ml Alexa Fluor 633-conjugated streptavidin in PBS-X (S-21375; Invitrogen) for 2 h. Sections were then mounted, counterstained with fluorescent Nissl blue, and coverslipped.

Confocal microscopy

Images of fluorescently stained sections were captured using a Zeiss LSM 710 scanning confocal microscope. Low-magnification images of 7-μm-optical thickness were taken using a 10×/0.45 objective lens (Plan-Apochromat; Carl Zeiss), 0.7× digital zoom, 1.58 μs pixel time, and 4× frame average at 1024 × 1024 resolution. High-magnification images of 1-μm-optical thickness were taken using a 63×/1.4 oil-immersion lens (Plan-Apochromat; Carl Zeiss), 3.15 μs pixel time, and 8× frame average at 512 × 512 resolution. The power of lasers was 0.4–0.6 mW, which did not induce obvious fading.

Image analysis

Raw data were opened using ZEN lite 2011 software (Carl Zeiss), and each image was exported as an 8-bit tiff file. Density and size of VGluT2 puncta were analyzed using the Analyze Particles command after autobinarization in ImageJ software (version 1.46). Thalamic neurons were counted manually using the Cell Counter plugin of ImageJ. The tdT-positive and -negative VGluT2 puncta in an image were automatically sorted by a macro in Photoshop (version 13.0; Adobe Systems) and then subjected to ImageJ analyses. VGluT2 puncta on soma of a thalamic neuron were counted manually in ImageJ. Neuropil VGluT2 puncta on a thalamic neuron were calculated by subtraction of somatic puncta from the average number of VGluT2 puncta per neuron in the image. For analyses in barreloid hollows and at septal regions, the ROIs for barreloid units were outlined using the tangential lines of the outer edges of circularly aligned thalamic neurons. This delineation was conducted only with the Nissl channel (independent of the tdTomato channel) of confocal images. The other area in the image was then defined as the ROI for the septal region. VGluT2 puncta in the two kinds of ROIs were analyzed. Images displayed with offline magnification were processed by upscaling and noise-reduction algorithms (Tomasi and Manduchi, 1998; Freedman and Fattal, 2011) in Windows software using GeForce technologies (GT 640; NVIDIA).

Statistical analysis

All values are given as means ± SD unless otherwise noted. Linear regression was performed by Igor Pro. Several statistical tests were performed depending on experimental designs (for details, see Results and figure legends). The significance level was set at $p < 0.05$. Excel statistics software (version 6.0; ESUMI) was applied for statistical tests.

Results

Formation and elimination of lemniscal synapses during postnatal development

The lemniscal synapse in the VPM reaches functional maturity by P16 in the mouse (Arsenault and Zhang, 2006). However, the big picture of developmental changes in lemniscal inputs onto a

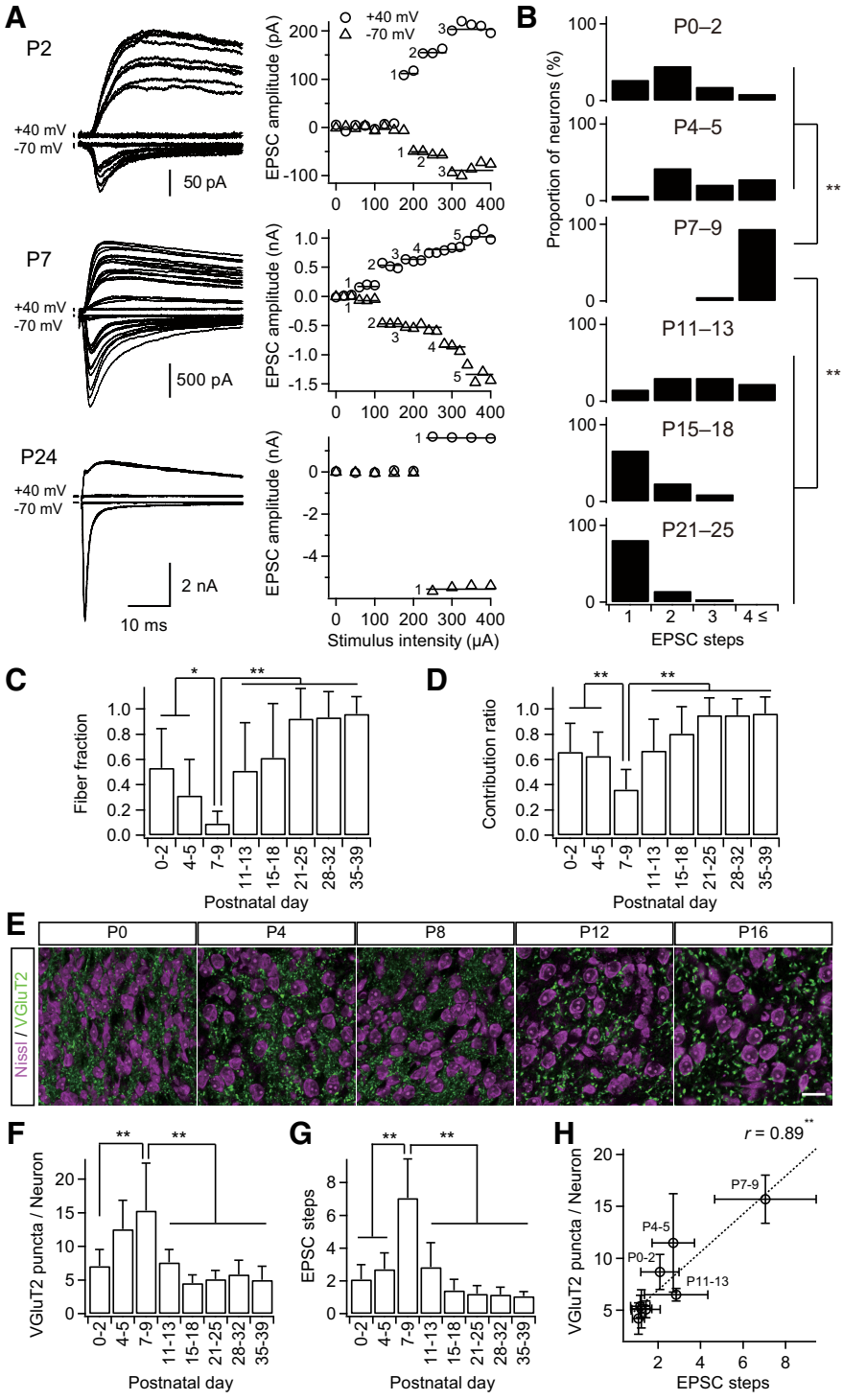

Figure 1. Formation and elimination of lemniscal synapses during postnatal development. ***A***, Developmental increase and decrease in number of innervating lemniscal fibers on a neuron in the whisker-related somatosensory thalamus. The number of innervating fibers was estimated by counting steps of lemniscal fiber-mediated EPSCs (lemniscal EPSCs) in response to increasing stimulus intensity applied to the lemniscal fiber bundle. Holding potentials were at +40 and −70 mV. Left, Several raw traces with different stimulus intensities are superimposed at each holding potential. Right, Search of EPSC steps. Peak amplitudes of lemniscal EPSCs are plotted against stimulus intensities. EPSC steps are indicated by horizontal bars and integers. ***B***, Distributions of thalamic neurons with different numbers of lemniscal inputs throughout postnatal development. ***C***, Developmental change in the fiber fraction, the first single fiber-meditated EPSC divided by the saturated currents of the same thalamic neuron. ***D***, Developmental change in the contribution ratio, the ratio of the largest single-fiber-mediated EPSC to the saturated currents of the same thalamic neuron. ***E***, Density of thalamic neurons decreased during the first postnatal week, whereas that of VGluT2 puncta decreased during the second but not first postnatal week in the V2 VPM. Scale bar, 20 μm. ***F***, VGluT2 puncta per thalamic neuron within 1 μm optical slice first increased and then decreased during postnatal development. ***G***, Electrophysiological evidence for the change in the number of lemniscal fiber inputs on a thalamic neuron. ***H***, Correlation between VGluT2 puncta per neuron and EPSC steps, structural and functional data on synapse formation and elimination. *r*, Pearson's correlation coefficient. Broken line is the regression line. Values are represented as mean + SD. n = 13–42 thalamic neurons for each developmental bin for electrophysiological data; n = 12–40 images from 6–8 mice for each developmental bin for structural data. Statistical significance was tested by multiple *t* test with Bonferroni correction after one-way ANOVA for ***B***, ***C***, ***D***, ***F***, and ***G***, and with the *t* test for noncorrelation for ***H***. $^{*}p < 0.05$; $^{**}p < 0.01$; two-tailed test.

VPM neuron during development is not yet fully understood. Therefore, we first examined the number of lemniscal fiber inputs directly on a thalamic neuron using whole-cell patch-clamp recordings throughout postnatal development (P0–P39). The number of lemniscal fiber inputs was assessed by a step-counting procedure, as described previously (Arsenault and Zhang, 2006; Takeuchi et al., 2012). During P0–P2 and P4–P5, one to four EPSC steps in a thalamic neuron were observed (Fig. 1*A*,*B*). The number of steps increased steeply after P6: P3–P11 on P7–P9. The steps then decreased gradually, so that almost all neurons (>80%) exhibited only a single EPSC step in an all-or-none fashion after P21 (Arsenault and Zhang, 2006; Takeuchi et al., 2012). The developmental change in the number of lemniscal EPSC steps was statistically significant ($p = 1.0 \times 10^{-47}$, one-way ANOVA, $F_{(7,187)} = 67.2$; Fig. 1*B*). The proportion of the first EPSC step to the saturated EPSC (fiber fraction; Hooks and Chen, 2006) dropped ~P6 (0.31 ± 0.29 on P4–P5, 0.09 ± 0.10 on P7–P9) and increased during the second and third postnatal weeks, similar to the number of EPSC steps ($p = 1.8 \times 10^{-23}$, one-way ANOVA, $F_{(7,144)} = 27.1$; Fig. 1*C*). In addition, the proportion of the largest EPSC to the saturated EPSC (contribution ratio) first decreased until P6 (0.63 ± 0.19 on P4–P5, 0.36 ± 0.16 on P7–P9), increased gradually, and eventually reached almost 1.0 by P21 ($p = 7.1 \times 10^{-24}$, one-way ANOVA, $F_{(7,144)} = 27.8$; Fig. 1*D*). This suggests that a single surviving lemniscal fiber is selectively strengthened during P9–P21. From these results, it may be concluded that the developmental refinement of lemniscal synapses consists of three distinct postnatal phases: barreloid pattern segregation (P0–P5), synapse formation (P6–P9), and synapse elimination (P9–P21).

To visualize the postnatal formation and elimination of lemniscal synapses, we examined entire synaptic terminals of lemniscal fibers by immunostaining type-2 ve-

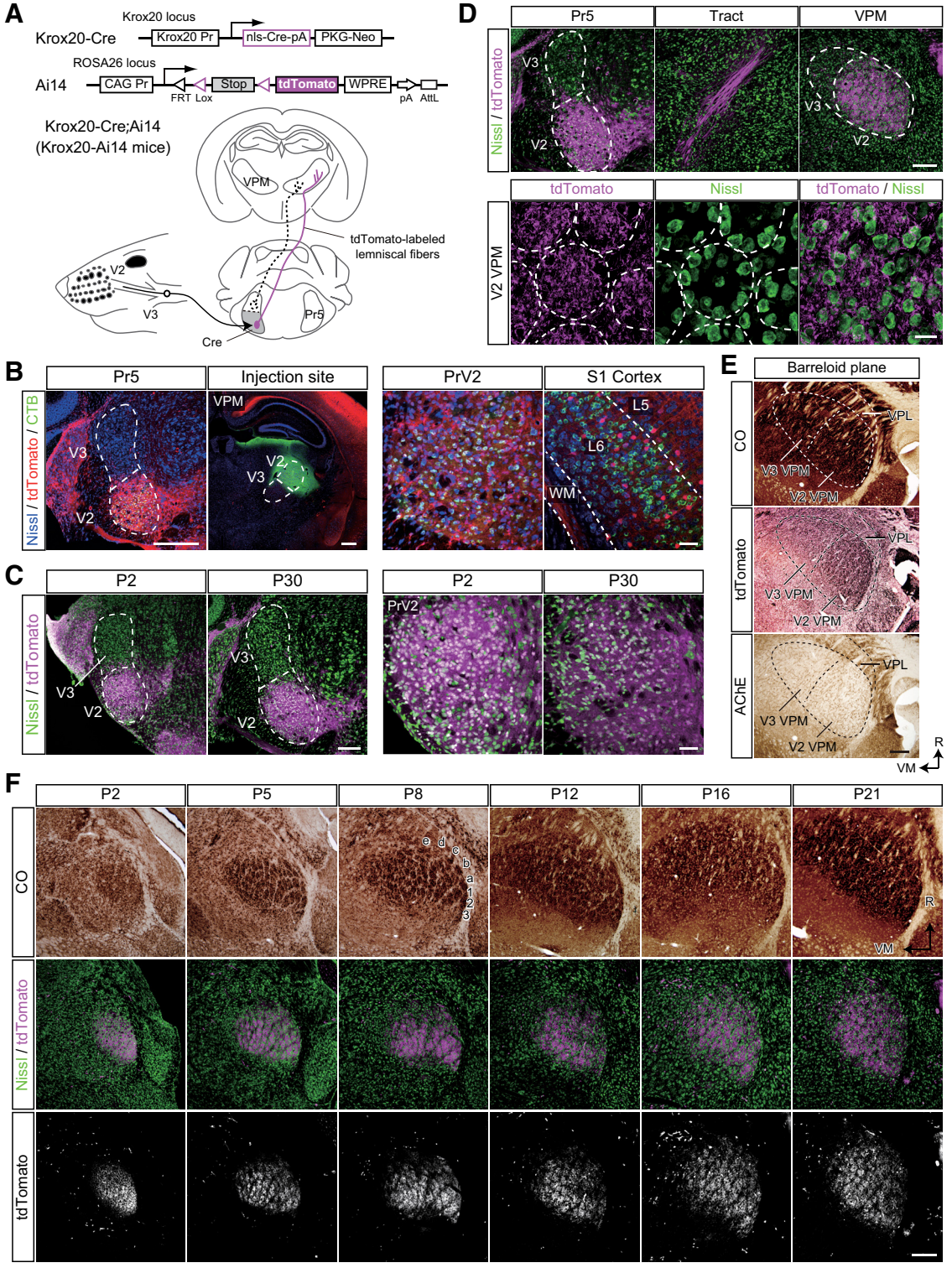

Figure 2. Genetic visualization of PrV2-origin lemniscal fibers. ***A***, Strategy for genetic visualization of PrV2-origin (maxillary Pr5-origin) lemniscal fibers. Top, Alleles of Krox20-Cre and Ai14 mice. These lines were crossed. Bottom, Schematic drawing of selective labeling of PrV2-origin lemniscal fibers with tdTomato. Selective expression of Cre recombinase in the V2 subregion of the Pr5 drives tdTomato in the double heterozygote (Krox20-Ai14 mice). ***B***, Krox20-Ai14 mice have strong tdTomato expression in almost all neurons in the PrV2 that project to the maxillary (V2) VPM. The layer-six neurons in the somatosensory cortex of Krox20-Ai14 mice that project to the V2 VPM do not colocalize with tdTomato expression. CTB was injected in the V2 VPM on P28. Scale bars: Left, 400 μm; Right, 50 μm. ***C***, Krox20-Ai14 mice have strong tdTomato expression in >85% of neurons in the PrV2, but not in the mandibular Pr5 (PrV3). Such expression was observed as early as P2. Scale bars: Left, 200 μm; Right, 50 μm. ***D***, tdTomato-labeled lemniscal fibers from PrV2 to the VPM in the P28 Krox20-Ai14 mouse. Top, tdTomato signals throughout lemniscal fibers. Scale bar, 200 μm. Bottom: Terminals of tdTomato-labeled lemniscal in the V2 VPM. Terminals were clustered in barreloid hollows surrounded ring-shaped alignment of thalamic neurons. Broken lines indicate barreloid units. Scale bar, 20 μm. ***E***, Serial thalamic sections of P28 Krox20-Ai14 mice were subjected to CO staining, tdTomato immunostaining, and acetylcholine esterase (AChE) staining. Cutting plane was perpendicular to the longest axis of barreloid units. tdTomato-immunoreactive puncta were confined to the most caudal region of the dorsolateral part of the VPM (V2 VPM). Scale bar, 200 μm. VPL, ventral posterolateral thalamic nucleus. ***F***, Time course of barreloid establishment in the Krox20-Ai14 mice. Scale bar, 200 μm. Top and Middle: Adjacent CO and fluorescent Nissl stained sections are shown. ***A***–***E***, Barreloid rows; ***1***-***3***, barreloid arcs. Bottom, Eight-bit signals in the tdTomato channel of confocal images shown in middle. R, rostral direction; VM, ventromedial direction.

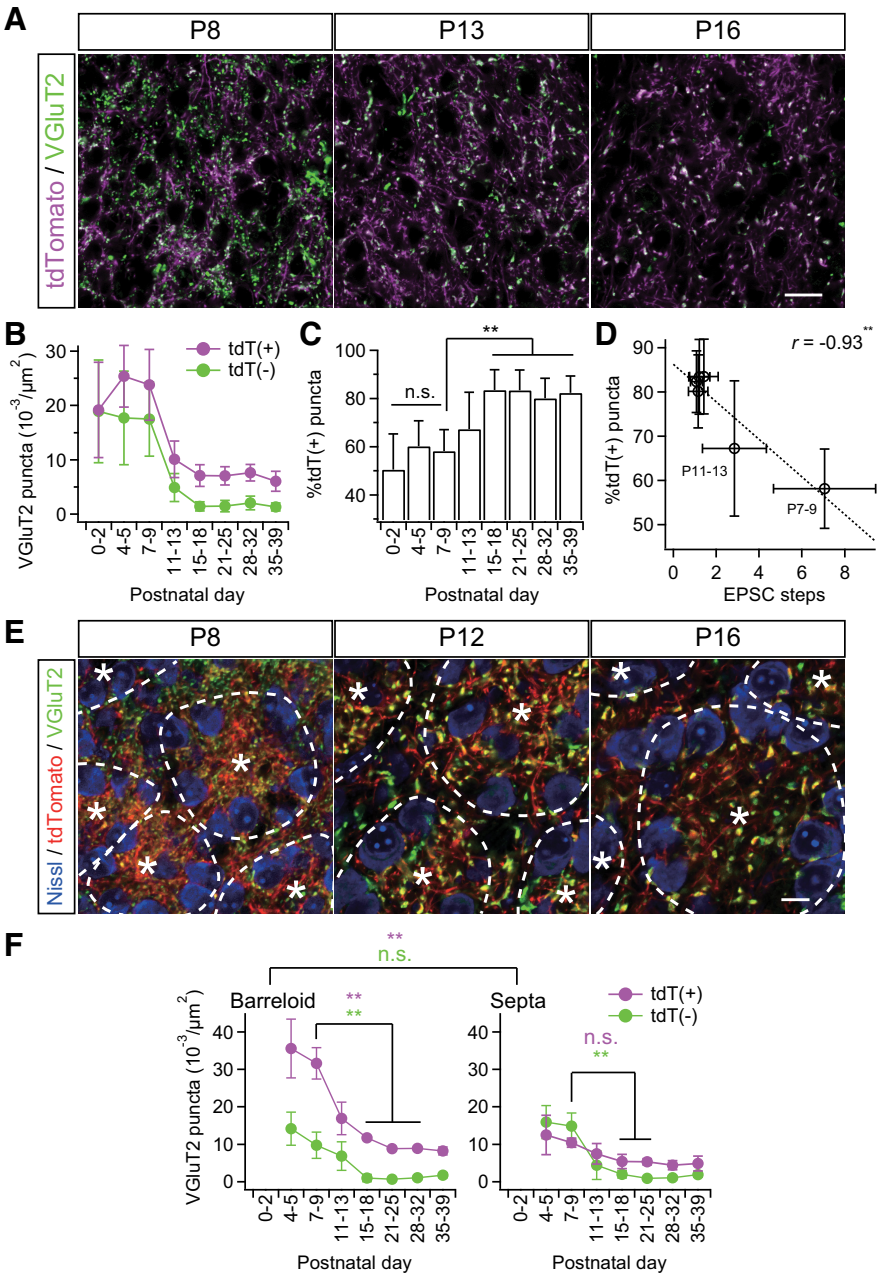

Figure 3. Somatotopic information is refined via fiber-origin-dependent synapse elimination. ***A***, VGluT2-immunostained thalamic sections of Krox20-Ai14 mice. PrV2-origin lemniscal boutons are characterized as tdTomato-positive VGluT2 puncta in white, whereas non-PrV2-origin afferent boutons as tdTomato-negative VGluT2 puncta in green. Scale bar, 20 μm. ***B***, tdT(+) = tdTomato-positive VGluT2 puncta; tdT(−) = tdTomato-negative VGluT2 puncta. Densities of both types of puncta decreased during the synapse elimination phase, but density of tdT(−) decreased more evidently. ***C***, Proportion of tdT-positive puncta significantly increased during the synapse elimination phase. ***D***, Proportion of tdT-positive puncta significantly correlated with EPSC steps after the onset of synapse elimination. *r*, Pearson's correlation coefficient. Broken line is the regression line. ***E***, Cross-sectional images of barreloid units surrounded by interbarreloid septa. *Center of the barreloid unit characterized by ring-shaped alignment of thalamic neurons and clustered lemniscal fibers within it. Broken lines indicate border of barreloid units and septal region. Inside of a barreloid unit is the barreloid hollow, whereas outside is the septal region. Scale bar, 10 μm. ***F***, Developmental changes in density of VGluT2 puncta in barreloid hollow and at interbarreloid septa. Values are represented as mean ± SD. n = 12–40 images from 6–9 mice for ***A***–***D*** and six images from three mice for ***E***–***F*** for each developmental bin. Statistical significance was tested with a *t* test for noncorrelation for ***D***. Differences between barreloid and septa were tested as a factor of two-way repeated ANOVA for ***F***. Differences between particular ages were tested by *post hoc* multiple *t* test with Bonferroni correction for ***C*** and ***F***. *$p < 0.05$; **$p < 0.01$; n.s., not significant, two-tailed test.

sicular glutamate transporter (VGluT2; Graziano et al., 2008) with neuron counterstaining (Fig. 1*E*). The number of VGluT2 puncta per neuron increased during the first postnatal week and then decreased dramatically in the subsequent week ($p = 2.3 \times 10^{-23}$, one-way ANOVA, $F_{(7,136)} = 27.7$; Fig. 1*F*). The time course of change in the number of VGluT2 puncta per neuron was very similar to that of EPSC steps (Fig. 1*F*,*G*). A significant correlation between VGluT2 puncta per neuron and EPSC steps was found during postnatal development ($r = 0.89$, $^{**}p = 2.9 \times 10^{-3}$, *t* test for noncorrelation, $t_6 = 4.84$; Fig. 1*H*). These results suggest that the change in the number of VGluT2 puncta per neuron coincides with the functional synapse elimination of lemniscal fibers on a neuron during postnatal development.

Genetic visualization of somatotopic information on lemniscal fibers

What is the difference between the lemniscal fibers that survive and those that do not? One possibility is that a fiber's fate depends on the origin of the somatotopic information. To test this possibility, we generated Krox20-Ai14 mice, in which entire PrV2-origin lemniscal fibers are specifically labeled with tdTomato (Fig. 2*A*). Krox20-Ai14 mice were generated by crossing a Krox20-Cre knock-in line (Voiculescu et al., 2000) and a Cre-dependent tdTomato reporter line (Ai14; Madisen et al., 2010). At P28–P30, almost all PrV2 neurons projecting to the maxillary VPM (92.6 ± 3.8%, eight sections from two mice) expressed tdTomato (Fig. 2*B*). Such a substantial recombination in PrV2 neurons had already been observed as early as P0–P2 and the extent of expression did not change throughout postnatal development (Fig. 2*C*). Other trigeminal nuclei did not have any Cre recombinase reactivity, as described previously (data not shown; Oury et al., 2006). Layer 6 neurons in the primary somatosensory cortex that were retrogradely labeled from the most caudal part of the dorsolateral region of the VPM (V2 VPM) also did not express tdTomato (Fig. 2*B*). Therefore, a subset of somatotopic information on lemniscal fibers in Krox20-Ai14 mice was specifically labeled with tdTomato, manifesting the specific connection between the PrV2 and the V2 VPM.

Strong tdTomato fluorescence in the mice was easily detected throughout axons of PrV2 neurons and their terminal boutons were evident in the VPM (Fig. 2*D*). In the somatosensory thalamus, tdTomato-labeled lemniscal fibers were observed only in the V2 VPM, but not in the ventromedial VPM (V3 VPM), indicating that labeling was limited only to maxillary lemniscal fibers (Fig. 2*E*). Developmentally, tdTomato-labeled lemniscal fibers in the V2 VPM were clearly segregated into the barreloid pattern (whisker map) between P2 and P4, in perfect register with CO-

reactive signals in the adjacent section (Fig. 2*F*). Although the CO pattern became more and more ambiguous as mice developed, the segregated pattern of tdTomato was always clear throughout development. In brief, these results indicate that entire PrV2-origin lemniscal fibers can be successfully visualized in Krox20-Ai14 mice, and these mice were useful for investigating somatotopic information during the developmental refinement of lemniscal synapses.

Somatotopic origin-dependent synapse pruning

To investigate somatotopic information on lemniscal fibers during functional synapse elimination, the thalamus of Krox20-Ai14 mice was stained with VGluT2. Then, tdTomato-positive (tdT-positive) and tdTomato-negative (tdT-negative) VGluT2-positive puncta in the whisker sensory thalamus were analyzed separately as synaptic boutons with distinct data. Before P9, a mixed picture of both tdT-negative and tdT-positive VGluT2 puncta was seen in the V2 VPM, even though the barreloid map had already been completed by P5 (Fig. 3*A*,*B*). During the synapse elimination phase, densities of both types of puncta decreased ($p < 1.0 \times 10^{-34}$ for both), but tdT-negative puncta decreased more drastically than tdT-positive puncta. As a result, the proportion of tdT-positive puncta increased significantly ($p = 3.3 \times 10^{-20}$, one-way ANOVA, $F_{(7,138)} = 22.6$; Fig. 3*C*), and the proportion of tdT-positive puncta was negatively correlated with the number of EPSC steps during the synapse elimination phase ($r = -0.93$, $^{**}p = 6.0 \times 10^{-3}$, *t* test for noncorrelation, $t_4 = 5.33$; Fig. 3*D*). These results suggest that terminals of PrV2-origin lemniscal fibers were preferentially retained in the whisker sensory thalamus via developmental synapse elimination.

In light of the barreloid architecture, each barreloid unit is composed of lemniscal fiber terminals clustered in the central hollow and thalamic neurons along the wall of the unit (Van der Loos, 1976; Belford and Killackey, 1979; Yamakado, 1985). We found that tdT-positive VGluT2 puncta were always dense inside a barreloid unit (barreloid hollow) and sparse outside (interbarreloid septa; $^{**}p = 1.5 \times 10^{-18}$, two-way repeated ANOVA, $F_{(1,83)} = 142.54$; Fig. 3*E*,*F*), which is consistent with previous reports of PrV-origin lemniscal fiber terminals (Williams et al., 1994; Veinante and Deschênes, 1999). In contrast, tdT-negative VGluT2 puncta were distributed uniformly both inside and outside of barreloid units ($p = 2.5 \times 10^{-1}$, $F_{(1,83)} = 1.36$). Before synapse elimination, tdT-positive VGluT2 puncta were already more predominant than tdT-negative puncta inside barreloid units, but not yet outside. During synapse elimination, tdT-positive puncta decreased much more drastically inside, but only

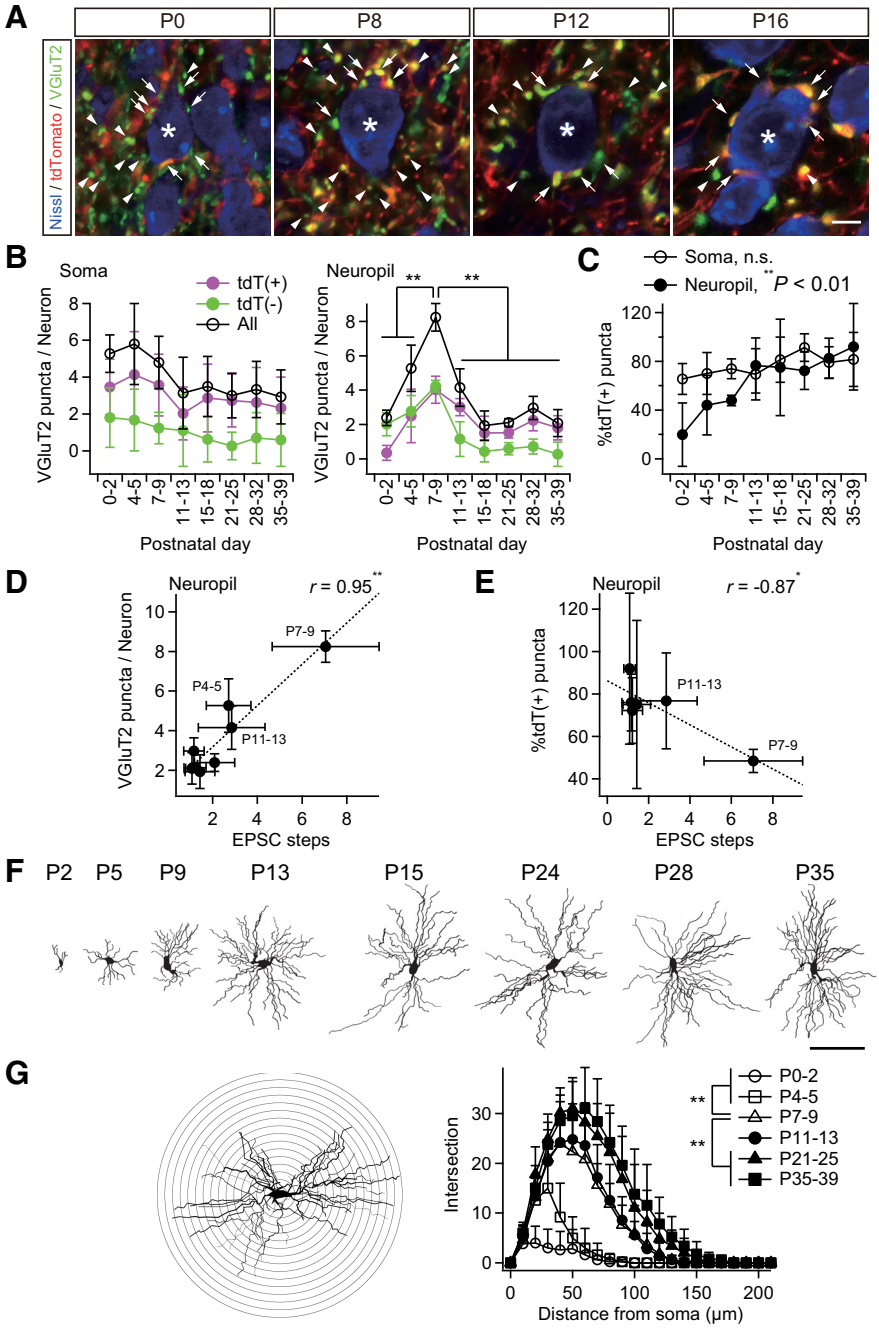

Figure 4. Somatotopic information is refined in neuropil rather than on the soma. ***A***, Analysis of somatic and neuropil puncta on a particular thalamic neuron. Somatic puncta were counted directly as shown. The number of neuropil puncta was calculated by subtracting somatic puncta on the neuron from the average number of puncta per neuron in the image. *Analyzed neuron; arrows, somatic puncta; arrowheads, neuropil puncta (quarter). Scale bar, 5 μm. ***B***, The number of neuropil puncta per neuron changed dramatically during development, whereas that of somatic puncta did not. ***C***, Proportion of tdT-positive neuropil puncta increased significantly during development. ***D***, Neuropil puncta per neuron correlated well with steps of lemniscal EPSCs. *r*, Pearson's correlation coefficient. Broken line is the regression line. ***E***, Proportion of tdT-positive neuropil puncta correlated well with steps of lemniscal EPSCs after the onset of the synapse elimination phase. ***F***, Projection images of biocytin-labeled thalamic neurons after acute patch-clamp recordings. Scale bar, 100 μm. ***G***, Sholl-analysis of dendrites of thalamic neurons using a Neurolucida system. Dendritic complexity increased significantly during the synapse formation and elimination phases. Bin was 10 μm. Values are represented as mean + SD. $n = 30$ thalamic neurons in six images from three mice for ***A***–***E*** and five thalamic neurons for ***F***–***G*** for each developmental bin. Statistical significance was tested by Bonferroni correction after one-way ANOVA for ***B***, one-way ANOVA for ***C***, *t* test for noncorrelation for ***D*** and ***E***, and multiple *t* test with Bonferroni correction after two-way repeated ANOVA for ***G***. $^{*}p < 0.05$; $^{**}p < 0.01$; n.s., not significant, two-tailed test.

moderately outside (inside: $^{**}p < 0.01$, $t_{10} = 8.76$; outside: $p > 0.05$, $t_{10} = 2.24$, *post hoc* multiple *t* test with Bonferroni correction). Conversely, tdT-negative VGluT2 puncta decreased equally both inside and outside ($^{**}p < 0.01$, $t_{10} > 8.13$ for both). Therefore, as a result of the distinct elimination, the whisker pattern by PrV2-origin lemniscal terminals was clearly sculpted out from non-PrV2-origin afferent terminals.

VPM neurons receive afferent inputs both on dendrites and on the soma (Peschanski et al., 1984; Liu et al., 1995). To clarify where somatotopic refinement via synapse elimination occurs, we next investigated somatic and neuropil VGluT2 puncta in the developing V2 VPM of Krox20-Ai14 mice. The number of somatic puncta per neuron did not change much developmentally (Fig. 4*A*,*B*). In contrast, the number of neuropil puncta first increased and then decreased, which is consistent with developmental changes of EPSC steps (Figs. 1, 4*A*,*B*). Neuropil puncta per neuron were well correlated with changes of EPSC steps ($r = 0.95$, $^{**}p = 3.9 \times 10^{-4}$, *t* test for noncorrelation, $t_6 = 7.10$; Fig. 4*D*), whereas somatic puncta were not ($r = 0.47$, $p = 2.4 \times 10^{-1}$, $t_6 = 1.30$). This result implies that the change in EPSC steps reflects the change in wiring in neuropil. Importantly, tdT-negative neuropil puncta decreased more drastically than tdT-positive neuropil puncta did during synapse elimination (Fig. 4*B*). Therefore, the proportion of tdT-positive neuropil puncta rose significantly ($^{**}p = 3.6 \times 10^{-4}$, one-way ANOVA, $F_{(7,40)} = 5.1$; Fig. 4*C*), but that of somatic puncta ($p = 1.5 \times 10^{-1}$, $F_{(7,40)} = 1.6$) did not. In addition, the change in the proportion of tdT-positive neuropil puncta was well correlated with the change in the number of EPSC steps ($r = -0.87$, $^{*}p = 2.6 \times 10^{-2}$, *t* test for noncorrelation, $t_4 = 3.47$; Fig. 4*E*), but the change in the proportion of tdT-positive somatic puncta was not ($r = -0.55$, $p = 2.5 \times 10^{-1}$, $t_4 = 1.33$). The remodeling of neuropil puncta coincided with dendritic growth; dendrites of a thalamic neuron grew drastically in the synapse formation and elimination phases ($^{**}p < 0.01$, *post hoc* multiple *t* test with Bonferroni correction, $t_6 > 3.04$; Fig. 4*F*,*G*). In addition, almost all of the VGluT2 puncta colocalized with PSD95 and/or GluA3 (major AMPA receptor subunit at lemniscal synapses; Fig. 5). Therefore, it is highly likely that neuropil puncta are dendritic boutons and that the somatotopic refinement is achieved via elimination of dendritic boutons rather than somatic boutons.

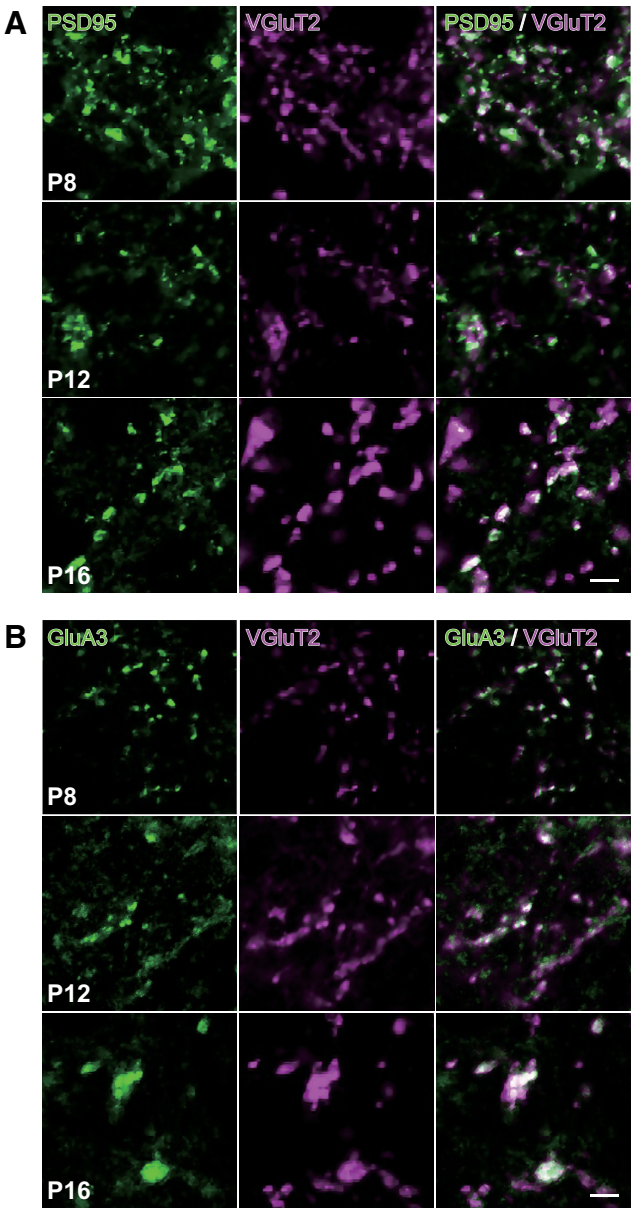

Figure 5. VGluT2 immunoreactivity colocalized with PSD95 and GluA3 immunoreactivities. Representative images of whisker sensory thalamic sections double immunostained for VGluT2 and PSD95 (***A***) or GluA3 (***B***). VGluT2-immunoreactive puncta colocalized well with intense signals of PSD95 and GluA3. Scale bars, 5 μm.

Strengthening of tdT-positive lemniscal synapses during postnatal development

Surviving synapses are generally strengthened with synapse elimination. This maturation of synapses is marked by the size of synaptic terminals and an increase in the amplitude of miniature EPSCs (mEPSCs; Sätzler et al., 2002; Sakaba et al., 2002; Rollenhagen and Lübke, 2006). Therefore, we investigated the size of tdT-positive/tdT-negative VGluT2-immunoreactive puncta during development. VGluT2 puncta complexes with PSD95 and/or GluA3 all grew to a large size throughout development (Fig. 5), suggesting that the size of VGluT2 puncta reflects the synaptic strength. VGluT2 puncta grew more than twofold in size during the synapse elimination phase ($p = 3.2 \times 10^{-36}$, one-way ANOVA, $F_{(7,138)} = 53.4$; Fig. 6*A*,*B*). In particular, tdT-positive puncta grew much larger compared with tdT-negative puncta. Consistent with the developmental size increase of VGluT2 puncta, the amplitude of miniature lemniscal EPSCs also increased progressively and almost doubled across the synapse elimination phase ($p = 1.1 \times 10^{-12}$, $F_{(7,55)} = 19.2$; Fig. 6*C*–*E*), whereas the mean interevent intervals did not change throughout development (range: $0.6–1.3 \times 10^{-2}$ s, $p = 1.1 \times 10^{-1}$, $F_{(7,55)} = 1.8$). The increase in the amplitude of miniature lemniscal EPSCs was well correlated with the sizes of tdT-positive puncta ($r > 0.97$, $^{**}p < 3.1 \times 10^{-5}$, *t* test for noncorrelation, $t_6 > 11.1$; Fig. 6*F*, left). These results indicate that tdT-positive synapses are strengthened, both structurally and functionally, during the synapse elimination phase. In addition, the size of tdT-positive puncta was also correlated with the proportion of tdT-positive VGluT2 puncta during postnatal development ($r = 0.97$, $^{**}p = 8.3 \times 10^{-5}$, $t_6 = 9.4$; Fig. 6*G*). Therefore, synaptic strengthening and somatotopic refinement occur simultaneously during functional synapse elimination.

Sensory-experience-dependent somatotopic refinement via synapse elimination and synaptic strengthening

A previous study reported that developmental elimination of lemniscal synapses in the whisker sensory thalamus is dependent on whisker-mediated sensory experience (Wang and Zhang, 2008). Therefore, if somatotopic refinement is mediated by syn-

apse elimination, disrupted functional synapse elimination by somatosensory deprivation should affect somatotopic refinement. To test this hypothesis, we continuously deprived the Krox20-Ai14 mice of sensory experience at P12–P13 by repeatedly plucking out all large whiskers on the left snout (Fig. 7). First, we confirmed that the whisker deprivation disrupted developmental synapse elimination using Krox20-Ai14 mice (Fig. 7*A–D*). In the intact P16–P18 group, >80% of recorded neurons showed all-or-none lemniscal EPSCs in response to graded electrical stimulation to the lemniscal fiber bundle. Conversely, more than half of the neurons in the age-matched deprived group showed multiple steps of lemniscal EPSCs, indicating a delay in synapse elimination due to the lack of sensory experience ($^{*}p = 3.0 \times 10^{-2}$, Kolmogorov–Smirnov test, $D = 0.29$; Fig. 7*C*,*D*). Next, we examined the populations of tdT-positive and tdT-negative VGluT2 puncta in the whisker-deprived sensory thalamus in the same fashion. In the thalamus of P16–P18 intact mice, >80% of VGluT2-puncta were tdT positive; in contrast, many tdT-negative ones remained in the age-matched deprived group (Fig. 7*E*, left). In the deprived group, the density of tdT-negative VGluT2 puncta was higher than it was in the intact group and the density of tdT-positive ones was lower ($^{*}p < 0.05$, Student's *t* test, $t_{78} > 2.48$ for both; Fig. 7*F*). The total number of puncta between the two groups was not different. As a result, the proportion of tdT-positive puncta in the deprived group (75.3 ± 8.8%) was significantly smaller than that in the intact group (83.5 ± 8.4%; $p = 6.1 \times 10^{-5}$, $t_{78} = 4.24$), indicating that non-PrV2-origin fibers remained in the deprived, rather than the intact, group. The average number of EPSC steps in the deprived group, accordingly, also tended to be larger, which can be well explained by the correlation between the mean EPSC steps and the proportion of tdT-positive lemniscal puncta measured in the intact group (Fig. 7*H*). In addition, the size of tdT-positive VGluT2 puncta in the deprived group was significantly smaller ($^{**}p = 1.5 \times 10^{-5}$, $t_{78} = 4.63$; Fig. 7*E*, right, *G*), whereas tdT-negative puncta in the deprived group had a tendency to become larger ($p = 5.9 \times 10^{-2}$). Therefore, it appears that sensory-experience-dependent synaptic strengthening could affect the competition between PrV2-origin and non-PrV2-origin afferent terminals during postnatal development. These results strongly suggest that somatotopic refinement is mediated by functional synapse elimination and that the process is at least partially dependent on sensory experience.

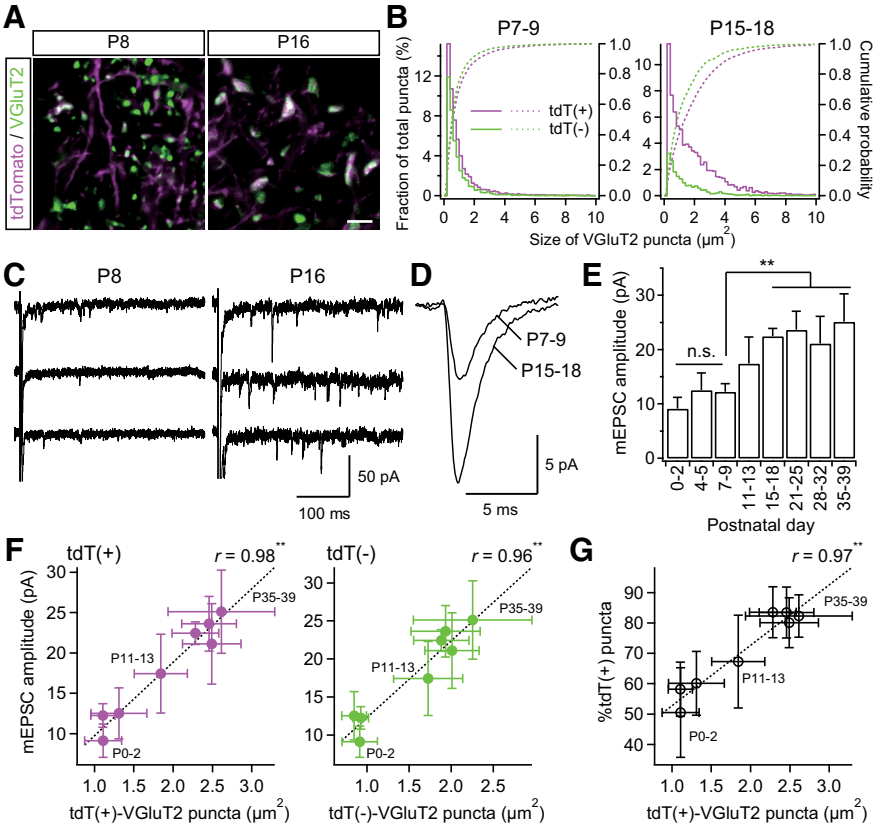

Figure 6. Strengthening of PrV2-origin lemniscal synapses during postnatal development. ***A***, VGluT2-immunoreactive puncta in the V2 VPM before and after synapse elimination. Scale bar, 5 μm. ***B***, Distributions and cumulative probabilities of tdT(+) and tdT(−) VGluT2 puncta before and after synapse elimination. Data from six and eight mice were pooled for P7–P9 and P15–P18, respectively. ***C***, Miniature lemniscal EPSCs before and after synapse elimination. Miniature lemniscal EPSCs were evoked in the modified ACSF with Sr^{2+} ions instead of Ca^{2+} ions, whereas lemniscal fibers were stimulated electrically. ***D***, Averaged miniature lemniscal EPSCs before and after synapse elimination. The numbers of averaged events were 489 and 763 for P7–P9 and P15–P18, respectively. ***E***, The mean amplitude of miniature lemniscal EPSCs of a neuron significantly increased during the synapse elimination phase. Analysis was conducted on 512–814 events at 6–10 neurons from three mice for each developmental bin. ***F***, The amplitude of miniature lemniscal EPSCs correlated well with the size of VGluT2 puncta during development. *r*, Pearson's correlation coefficient. Broken line is the regression line. ***G***, Proportion of tdT-positive puncta correlated well with the size of tdT-positive puncta during development. Values are represented as mean ± SD. Statistical significance was tested by multiple *t* test with Bonferroni correction after one-way ANOVA for developmental changes in ***E*** and *t* test for noncorrelation for ***F*** and ***G***. $^{**}p < 0.01$; n.s., not significant, two-tailed test.

Large-scale somatotopic refinement during functional synapse elimination in the whisker sensory thalamus

Given the result that the whisker sensory thalamus (V2 VPM) has a large number of tdT-negative VGluT2 puncta before synapse elimination is completed, we investigated the origins of these fiber terminals before and after developmental synapse elimination. A solution containing CTB, a retrograde tracer, was locally injected into the V2 VPM of Krox20-Ai14 mice. Suitable volume, concentration, and stereotaxic coordinates were determined so that the tracer solution was confined in the V2 VPM, where tdT-positive lemniscal fibers densely terminate (Fig. 2*B*). After synapse elimination (P18–P30), retrogradely labeled neurons were observed only in the PrV2, where CTB and tdTomato signals overlapped, and in the V2 interpolar subnucleus of spinal trigeminal nuclei (SpI), but not in the PrV3, V3 SpI, caudal subnucleus of spinal trigeminal nuclei, or dorsal column nuclei (DCN; Fig. 8, six mice). Interestingly, before the end of developmental synapse elimination (P13), PrV3, V3 SpI, and DCN were considerably labeled in addition to normal labeling in the PrV2 and V2 SpI (five mice). All of this ectopic labeling was similarly observed in the whisker-deprived mice (P18), in which developmental disappearance of tdT-negative VGluT2 puncta was disrupted (six mice). The retrogradely labeled neurons in such ectopic regions

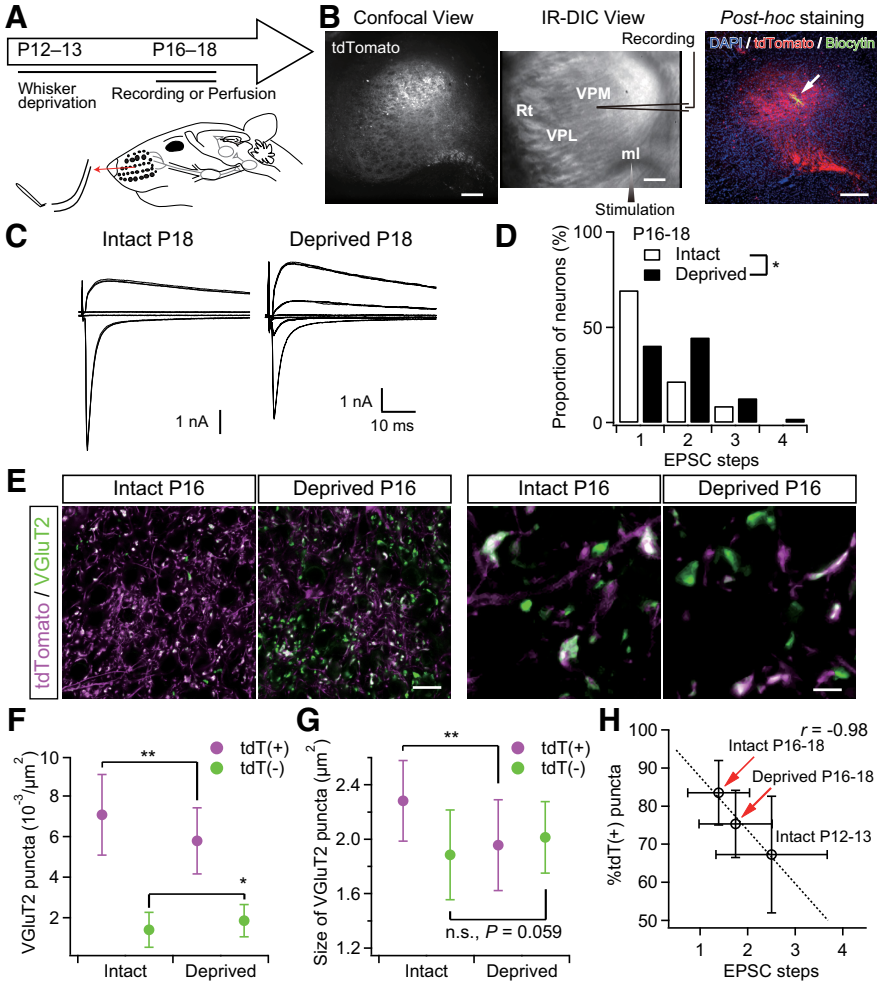

Figure 7. Sensory-experience-dependent somatotopic refinement via synapse elimination. ***A***, Experimental schedule and schematic view of whisker deprivation. ***B***, Acute slice patch-clamp recordings from Krox20-Ai14 mice. Clouds of tdT-positive terminals were observed in the dorsal part of the VPM via a confocal laser scanning unit and the whole-cell recordings were then made from thalamic neurons under the infrared-differential interference contrast (IR-DIC) viewing. After the recordings, slices were fixed and we confirmed that the recorded thalamic neurons had been in the clouds of tdTomato-positive lemniscal fiber terminals. The arrow indicates the recorded thalamic neuron. Scale bars, 200 μm. ml, Medial lemniscus; Rt, reticular nucleus of thalamus. ***C***, Representative traces of lemniscal EPSCs from intact and deprived mice under voltage-clamp conditions at +40 and −70 mV. Several raw traces with different stimulus intensities are superimposed at each holding potential. EPSCs from an intact mouse showed all-or-none responses, whereas those from a deprived mouse showed stepwise increments in amplitude. ***D***, Distributions of neurons with different numbers of steps of lemniscal EPSCs. $n = 46$ and 47 neurons of seven and nine mice for intact and deprived groups, respectively. ***E***, VGluT2-immunostained whisker-sensory thalamic sections of intact and deprived Krox20-Ai14 mice. Scale bars, 20 and 5 μm for left and right, respectively. ***F***, ***G***, Density and size of tdT(+)- and tdT(−)-VGluT2 puncta of intact and deprived Krox20-Ai14 mice. Forty images from 7–8 mice were analyzed for each group. ***H***, Proportion of tdT-positive puncta plotted against EPSC steps. Whisker deprivation at P12–P13 consistently disrupted synapse elimination and somatotopic refinement. *r*, Pearson's correlation coefficient. The broken line is the regression line. Values are represented as mean ± SD. Statistical significance was tested by Kolmogorov–Smirnov two-sample test for ***D*** and Student's *t* test for ***F*** and ***G***. $^*p < 0.05$; $^{**}p < 0.01$; n.s., not significant, two-tailed test.

were all tdT negative (Fig. 8). In addition, we did not observed ipsilateral labeling in any conditions. These results suggest that origins of tdT-negative puncta in the V2 VPM during the early postnatal development are V3 subregions of the trigeminal nuclei and DCN.

Discussion

In the present study, we visualized PrV2-origin lemniscal fibers using Krox20-Ai14 mice and combined anatomical analysis with functional analysis to shed more light on the relationship between topographical refinement and functional synapse elimination during development. Our data indicate that a large-scale somatotopic refinement underlies and is completed during the functional synapse elimination of lemniscal fibers in the mouse VPM. This somatotopic refinement occurs mainly in the neuropil, not on the soma. Moreover, blocking functional synapse elimination by sensory deprivation disturbed this somatotopic refinement, indicating that PrV2-dependent somatotopic refinement was accomplished at least partially by functional synapse elimination in a somatosensory-experience-dependent manner (Fig. 9).

We distinguished three phases of developmental lemniscal synapses in the VPM. First, during P0–P5, lemniscal fiber terminals align with barreloid patterns (Fig. 2; Belford and Killackey, 1979; Yamakado, 1985). Then, after the barreloid map forms, VPM neurons are innervated by many weak lemniscal fibers in the second phase, ~P6–P9 (Figs. 1, 4, 6). In the third phase, the functional synapse elimination phase (P9–P21), all but one lemniscal fiber onto each VPM neuron are eliminated and the remaining lemniscal fiber's synapses are stabilized and strengthened (Arsenault and Zhang, 2006; Wang and Zhang, 2008). We found high correlations between structural and functional synaptic parameters, such as the proportion of tdT-positive VGluT2 puncta versus the number of EPSC steps and the size of puncta versus the amplitude of mEPSCs during development. These results indicate that structural and functional synaptic refinements and synaptic maturations occur concurrently. More than 90% of PrV2 neurons expressed tdTomato throughout development in Krox20-Ai14 mice (Fig. 2*C*). Therefore, we were able to visualize PrV2-origin lemniscal boutons as tdT-positive puncta. Most notably in our study, we found that a large number of afferent fiber terminals innervated VPM neurons in a somatotopic-origin-independent manner during the first two phases, and then PrV2-origin lemniscal synapses survived selectively and non-PrV2-origin fiber synapses were eliminated during the synapse elimination phase. In the meantime, the amplitude of mEPSCs of a lemniscal fiber increased and boutons of PrV2-origin-lemniscal fibers grew preferentially in size (Fig. 6). These results strongly suggest that PrV2-origin somatotopic information in the VPM was refined and consolidated during synapse elimination. Interestingly, blocking functional synapse elimination by whisker deprivation resulted in impairment of somatotopic-origin-dependent refinement in the VPM. Therefore, functional synapse elimination promotes somatotopic refinement directly.

Functional synapse elimination has been studied extensively in various CNSs, including the retinogeniculate system, retino-

collicular synapses, medial nucleus of the trapezoid body to the lateral superior olive synapses, and climbing fiber-Purkinje cell synapses in the cerebellum (Kim and Kandler, 2003; Lu and Constantine-Paton, 2004; Kano and Hashimoto, 2009). In the lateral geniculate nucleus (LGN), electrophysiological examination has revealed that functional synapse elimination of retinogeniculate fibers occurs between P8 and P10 when the eye-specific segregation and retinotopic map are already completed and formed. Therefore, functional synapse elimination would not contribute directly to such a large-scale topographical segregation; instead, it may be responsible for the refinement at a finer circuit level on a single LGN neuron, such as the fine tuning of retinotopy and establishment of retinal ganglion cell type-specific circuits (Dhande et al., 2011; Hong and Chen, 2011). In contrast, in the mouse somatosensory system, we found that considerable tdT-negative puncta were present uniformly both inside and outside of barreloid units in the VPM during early developmental phases, although tdT-positive puncta were more dominant inside barreloid units. Then, tdT-negative puncta were eliminated selectively during the synapse elimination phase (Fig. 3). Our results in Figure 8 suggest that probable sources of such tdT-negative puncta during early postnatal phases are the PrV3, SpI, and DCN. This proposition is also supported by the following findings. First, these brainstem nuclei have high levels of VGluT2 protein and mRNA expressions (Boulland et al., 2004; Graziano et al., 2008). Second, VPM-derived axon collaterals could not be the source of tdT-negative boutons in the V2 VPM, because excitatory chemical connections between VPM neurons are very rare throughout development (Lee et al., 2010) and axon collaterals of biocytin-filled neurons in the VPM were not observed throughout development in our study. Lemniscal fibers from PrV3 innervate thalamic neurons in the vicinity of the V2 region in the VPM, but never break into the V2 region in the adult. SpI neurons projecting to the VPM have large receptive fields and their axons terminate in more distal dendrites of neurons in the VPM than do those from the Pr5 (Williams et al., 1994); they also usually terminate in the outside, instead of the core region, of barreloid units (Pierret et al., 2000; Veinante et al., 2000). DCN convey somatotopic information from body parts to the ventral posterolateral nucleus (Graziano et al., 2008).

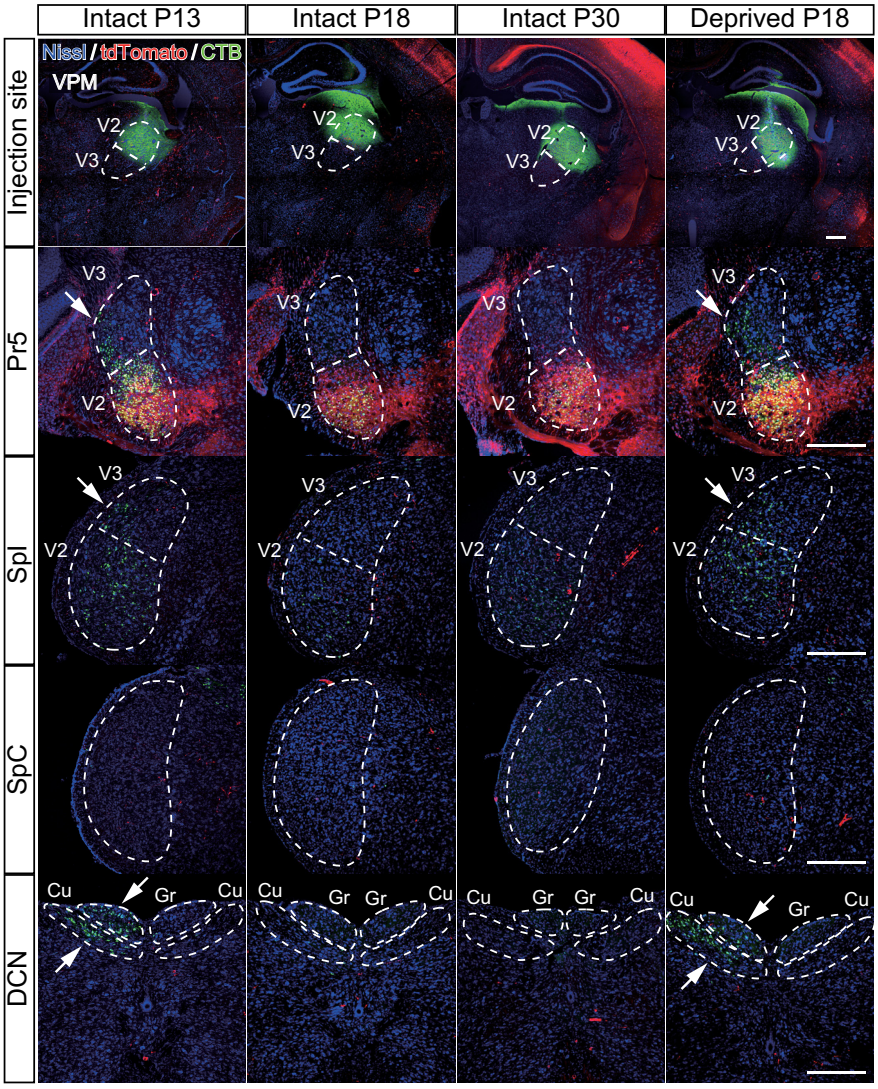

Figure 8. Developmental change in origin of afferent fibers innervating the whisker sensory thalamus. A CTB solution was injected to the right V2 VPM to retrogradely label the origin of nuclei of afferent fibers. Survival time was 2 d. Arrows indicate ectopic labeling. Three to six mice were examined for each group. Cu, Cuneate nucleus; Gr, gracile nucleus; SpC, caudal subnucleus of spinal trigeminal nuclei. Scale bars, 400 μm.

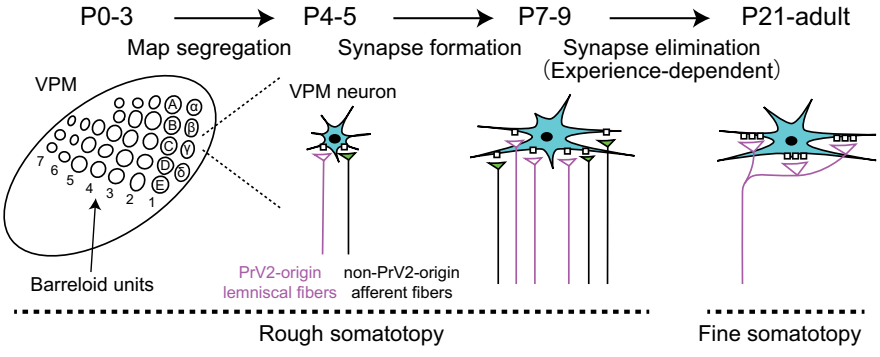

Figure 9. Schema of postnatal development of the whisker sensory thalamus of mice. During P0–P5, the afferent fibers and VPM neurons forms the whisker pattern. Just after the map formation, VPM relay neurons (neurons in cyan) receive intermingled innervations of PrV2-origin lemniscal fibers (magenta fibers with white terminals) and non-PrV2-origin afferent fibers (black fibers with green terminals). During P6–P9, many afferent fibers newly innervate VPM neurons with rough somatotopy. After P9, redundant, non-PrV2-origin afferent fibers are selectively and experience,dependently eliminated. By P21, the fine somatotopy with mono-innervations of PrV2-origin lemniscal fibers are established in the V2 VPM. Left, A–E, Barreloid rows; 1–7, barreloid arcs; α–δ, barreloid units representing the four posterior whiskers.

Therefore, superfluous axons of these nuclei to the VPM may be eliminated selectively during the synapse elimination phase, thereby allowing large-scale somatotopic information to be refined during synapse elimination, even after the completion of barreloid pattern formation. Consistent with these results, immature VPM neurons in rats are known to have broad receptive fields, including other body parts such as the shoulder and forelimbs, during early developmental stages, whereas mature ones have receptive fields from only very restricted areas in the face (Nicolelis et al., 1991). A recent study has revealed that neurons in the primary somatosensory cortex of juvenile rats also have large receptive fields spanning whiskers and forelimbs or hindlimbs even after the cortical architectonic map of the whole body is clearly established (P5–P15; Seelke et al., 2012). The cortical neurons then become representative of a small body part after P20 (Seelke et al., 2012), when thalamic somatotopic refinement via synapse elimination is already complete (Fig. 3). Therefore, thalamic synapse elimination may contribute not only to thalamic, but also to cortical somatotopic representations.

Neural activity plays a pivotal role in functional synapse elimination and topographical organization (Thompson, 1983; Sanes and Takács, 1993; Katz and Shatz, 1996; Nguyen and Lichtman, 1996; Buffelli et al., 2003; Lorenzetto et al., 2009; Favero et al., 2012). For example, blocking retinal waves, the spontaneous activity of retinal ganglion cells, disrupts eye segregation and developmental pruning of retinogeniculate afferents on a neuron in the LGN (Grubb et al., 2003; Hooks and Chen, 2006; Huberman, 2007). Sensory experience also drives synapse elimination in the superior colliculus (Lu and Constantine-Paton, 2004). In the VPM, we found that whisker deprivation disrupted the selective elimination of non-PrV2-origin afferent boutons and favored the strengthening of PrV2-origin synapses, indicating that somatosensory experience promotes not only functional synapse elimination but also somatotopic refinement (Fig. 7). Adenylate cyclase 1, GluA3, and GluN1 are responsible for experience-dependent synaptic strengthening and/or elimination of lemniscal synapses in the VPM (Wang et al., 2011a; Wang et al., 2011b; Zhang et al., 2013). Therefore, these molecules may also contribute to the somatotopic refinement in the VPM. Conversely, whisker deprivation alone did not completely abolish functional synapse elimination, synaptic strengthening, or associated somatotopic refinement (Fig. 7*H*), further suggesting that additional factors such as spontaneous neuronal activity and/or other signal molecules may be needed in this process.

In the present study, we found that developmental changes in the proportion of tdT-positive and tdT-negative puncta in the VPM occurred predominantly in the neuropil. It is highly likely that the neuropil puncta in the VPM are boutons on dendrites of relay neurons for the following reasons. First, neurons in the somatosensory thalamus of mice are nearly homologous to relay (principle) neurons (Arcelli et al., 1997). Second, immunoreactivity of VGluT2 colocalized with that of PSD95/GluA3 (Fig. 5). Third, it has been reported that the main target of VGluT2-immunoreactive terminals (lemniscal terminals) in the VPM is proximal dendrites of VPM neurons in the ultrastructural level (Peschanski et al., 1984; Liu et al., 1995; Graziano et al., 2008). Because dendrites of a VPM neuron grow drastically in the synapse elimination phase (Fig. 4*F*,*G*), the remodeling of dendritic synapses may be crucial for integrating and refining inputs from different sources, thereby fine tuning the somatotopy. Recent long-term *in vivo* imaging studies using two-photon microscopy have revealed drastic remodeling, such as synapse formation and elimination, on cortical dendritic synapses during development and experience-dependent plasticity (Elston et al., 2009; Holtmaat and Svoboda, 2009). In the early developmental stage, cortical spines appear and disappear at a rapid rate and spine densities in the mouse cortex increase, followed by a period of synapse elimination. In addition, cortical boutons are remodeled dynamically in a cell-origin-specific manner on dendrites during development (Portera-Cailliau et al., 2005; De Paola et al., 2006). Therefore, it is conceivable that such remodeling may also occur on dendrites of VPM neurons during development. However, current techniques are not adaptable to deeper brain regions such as the thalamus without an invasive approach. Nevertheless, we still detected a high degree of correlation between structural and functional developmental changes by collecting VPM samples sequentially from different mice. Dynamic *in vivo* images of synaptic structure and functional and topographic data from intact deeper brain regions will be needed for a complete understanding of the development of neuronal circuits.

References

Arcelli P, Frassoni C, Regondi MC, De Biasi S, Spreafico R (1997) GABAergic neurons in mammalian thalamus: a marker of thalamic complexity? Brain Res Bull 42:27–37. CrossRef Medline

Arsenault D, Zhang ZW (2006) Developmental remodelling of the lemniscal synapse in the ventral basal thalamus of the mouse. J Physiol 573:121–132. CrossRef Medline

Belford GR, Killackey HP (1979) The development of vibrissae representation in subcortical trigeminal centers of the neonatal rat. J Comp Neurol 188:63–74. CrossRef Medline

Boulland JL, Qureshi T, Seal RP, Rafiki A, Gundersen V, Bergersen LH, Fremeau RT Jr, Edwards RH, Storm-Mathisen J, Chaudhry FA (2004) Expression of the vesicular glutamate transporters during development indicates the widespread corelease of multiple neurotransmitters. J Comp Neurol 480:264–280. CrossRef Medline

Buffelli M, Burgess RW, Feng G, Lobe CG, Lichtman JW, Sanes JR (2003) Genetic evidence that relative synaptic efficacy biases the outcome of synaptic competition. Nature 424:430–434. CrossRef Medline

Castro-Alamancos MA (2002) Properties of primary sensory (lemniscal) synapses in the ventrobasal thalamus and the relay of high-frequency sensory inputs. J Neurophysiol 87:946–953. Medline

De Paola V, Holtmaat A, Knott G, Song S, Wilbrecht L, Caroni P, Svoboda K (2006) Cell type-specific structural plasticity of axonal branches and boutons in the adult neocortex. Neuron 49:861–875. CrossRef Medline

Dhande OS, Hua EW, Guh E, Yeh J, Bhatt S, Zhang Y, Ruthazer ES, Feller MB, Crair MC (2011) Development of single retinofugal axon arbors in normal and β2 knock-out mice. J Neurosci 31:3384–3399. CrossRef Medline

Elston GN, Oga T, Fujita I (2009) Spinogenesis and pruning scales across functional hierarchies. J Neurosci 29:3271–3275. CrossRef Medline

Favero M, Busetto G, Cangiano A (2012) Spike timing plays a key role in synapse elimination at the neuromuscular junction. Proc Natl Acad Sci U S A 109:E1667–E1675. CrossRef Medline

Freedman G, Fattal R (2011) Image and video upscaling from local self-examples. ACM Trans Graph 30:1–11. CrossRef

Fukaya M, Watanabe M (2000) Improved immunohistochemical detection of postsynaptically located PSD-95/SAP90 protein family by protease section pretreatment: a study in the adult mouse brain. J Comp Neurol 426:572–586. CrossRef Medline

Graziano A, Liu XB, Murray KD, Jones EG (2008) Vesicular glutamate transporters define two sets of glutamatergic afferents to the somatosensory thalamus and two thalamocortical projections in the mouse. J Comp Neurol 507:1258–1276. CrossRef Medline

Grubb MS, Rossi FM, Changeux JP, Thompson ID (2003) Abnormal functional organization in the dorsal lateral geniculate nucleus of mice lacking the β2 subunit of the nicotinic acetylcholine receptor. Neuron 40:1161–1172. CrossRef Medline

Haidarliu S, Ahissar E (2001) Size gradients of barreloids in the rat thalamus. J Comp Neurol 429:372–387. CrossRef Medline

Holtmaat A, Svoboda K (2009) Experience-dependent structural synaptic plasticity in the mammalian brain. Nat Rev Neurosci 10:647–658. CrossRef Medline

Honda Y, Sasaki H, Umitsu Y, Ishizuka N (2012) Zonal distribution of per-

forant path cells in layer III of the entorhinal area projecting to CA1 and subiculum in the rat. Neurosci Res 74:200–209. CrossRef Medline
Hong YK, Chen C (2011) Wiring and rewiring of the retinogeniculate synapse. Curr Opin Neurobiol 21:228–237. CrossRef Medline
Hooks BM, Chen C (2006) Distinct roles for spontaneous and visual activity in remodeling of the retinogeniculate synapse. Neuron 52:281–291. CrossRef Medline
Huberman AD (2007) Mechanisms of eye-specific visual circuit development. Curr Opin Neurobiol 17:73–80. CrossRef Medline
Iwasato T, Nomura R, Ando R, Ikeda T, Tanaka M, Itohara S (2004) Dorsal telencephalon-specific expression of Cre recombinase in PAC transgenic mice. Genesis 38:130–138. CrossRef Medline
Kano M, Hashimoto K (2009) Synapse elimination in the central nervous system. Curr Opin Neurobiol 19:154–161. CrossRef Medline
Katz LC, Shatz CJ (1996) Synaptic activity and the construction of cortical circuits. Science 274:1133–1138. CrossRef Medline
Kim G, Kandler K (2003) Elimination and strengthening of glycinergic/GABAergic connections during tonotopic map formation. Nat Neurosci 6:282–290. CrossRef Medline
Kuramoto E, Furuta T, Nakamura KC, Unzai T, Hioki H, Kaneko T (2009) Two types of thalamocortical projections from the motor thalamic nuclei of the rat: a single neuron-tracing study using viral vectors. Cereb Cortex 19:2065–2077. CrossRef Medline
Land PW, Buffer SA Jr, Yaskosky JD (1995) Barreloids in adult rat thalamus: three-dimensional architecture and relationship to somatosensory cortical barrels. J Comp Neurol 355:573–588. CrossRef Medline
Lee SC, Cruikshank SJ, Connors BW (2010) Electrical and chemical synapses between relay neurons in developing thalamus. J Physiol 588:2403–2415. CrossRef Medline
Liu XB, Honda CN, Jones EG (1995) Distribution of four types of synapse on physiologically identified relay neurons in the ventral posterior thalamic nucleus of the cat. J Comp Neurol 352:69–91. CrossRef Medline
Lorenzetto E, Caselli L, Feng G, Yuan W, Nerbonne JM, Sanes JR, Buffelli M (2009) Genetic perturbation of postsynaptic activity regulates synapse elimination in developing cerebellum. Proc Natl Acad Sci U S A 106:16475–16480. CrossRef Medline
Lu W, Constantine-Paton M (2004) Eye opening rapidly induces synaptic potentiation and refinement. Neuron 43:237–249. CrossRef Medline
Madisen L, Zwingman TA, Sunkin SM, Oh SW, Zariwala HA, Gu H, Ng LL, Palmiter RD, Hawrylycz MJ, Jones AR, Lein ES, Zeng H (2010) A robust and high-throughput Cre reporting and characterization system for the whole mouse brain. Nat Neurosci 13:133–140. CrossRef Medline
Miyata M, Imoto K (2006) Different composition of glutamate receptors in corticothalamic and lemniscal synaptic responses and their roles in the firing responses of ventrobasal thalamic neurons in juvenile mice. J Physiol 575:161–174. CrossRef Medline
Miyazaki T, Fukaya M, Shimizu H, Watanabe M (2003) Subtype switching of vesicular glutamate transporters at parallel fibre-Purkinje cell synapses in developing mouse cerebellum. Eur J Neurosci 17:2563–2572. CrossRef Medline
Nakamura Y, Nakamura K, Matsumura K, Kobayashi S, Kaneko T, Morrison SF (2005) Direct pyrogenic input from prostaglandin EP3 receptor-expressing preoptic neurons to the dorsomedial hypothalamus. Eur J Neurosci 22:3137–3146. CrossRef Medline
Nguyen QT, Lichtman JW (1996) Mechanism of synapse disassembly at the developing neuromuscular junction. Curr Opin Neurobiol 6:104–112. CrossRef Medline
Nicolelis MA, Chapin JK, Lin RC (1991) Thalamic plasticity induced by early whisker removal in rats. Brain Res 561:344–349. CrossRef Medline
Oury F, Murakami Y, Renaud JS, Pasqualetti M, Charnay P, Ren SY, Rijli FM (2006) Hoxa2- and rhombomere-dependent development of the mouse facial somatosensory map. Science 313:1408–1413. CrossRef Medline
Peschanski M, Lee CL, Ralston HJ 3rd (1984) The structural organization of the ventrobasal complex of the rat as revealed by the analysis of physiologically characterized neurons injected intracellularly with horseradish peroxidase. Brain Res 297:63–74. CrossRef Medline
Pierret T, Lavallée P, Deschênes M (2000) Parallel streams for the relay of vibrissal information through thalamic barreloids. J Neurosci 20:7455–7462. Medline
Portera-Cailliau C, Weimer RM, De Paola V, Caroni P, Svoboda K (2005) Diverse modes of axon elaboration in the developing neocortex. PLoS Biol 3:e272. CrossRef Medline
Purves D, Lichtman JW (1980) Elimination of synapses in the developing nervous system. Science 210:153–157. CrossRef Medline
Rollenhagen A, Lübke JH (2006) The morphology of excitatory central synapses: from structure to function. Cell Tissue Res 326:221–237. CrossRef Medline
Sakaba T, Schneggenburger R, Neher E (2002) Estimation of quantal parameters at the calyx of Held synapse. Neurosci Res 44:343–356. CrossRef Medline
Sanes DH, Takács C (1993) Activity-dependent refinement of inhibitory connections. Eur J Neurosci 5:570–574. CrossRef Medline
Sätzler K, Söhl LF, Bollmann JH, Borst JG, Frotscher M, Sakmann B, Lübke JH (2002) Three-dimensional reconstruction of a calyx of Held and its postsynaptic principal neuron in the medial nucleus of the trapezoid body. J Neurosci 22:10567–10579. Medline
Seelke AM, Dooley JC, Krubitzer LA (2012) The emergence of somatotopic maps of the body in S1 in rats: the correspondence between functional and anatomical organization. PLoS One 7:e32322. CrossRef Medline
Seitanidou T, Schneider-Maunoury S, Desmarquet C, Wilkinson DG, Charnay P (1997) Krox-20 is a key regulator of rhombomere-specific gene expression in the developing hindbrain. Mech Dev 65:31–42. CrossRef Medline
Sugitani M, Yano J, Sugai T, Ooyama H (1990) Somatotopic organization and columnar structure of vibrissae representation in the rat ventrobasal complex. Exp Brain Res 81:346–352. Medline
Takeuchi Y, Yamasaki M, Nagumo Y, Imoto K, Watanabe M, Miyata M (2012) Rewiring of afferent fibers in the somatosensory thalamus of mice caused by peripheral sensory nerve transection. J Neurosci 32:6917–6930. CrossRef Medline
Thompson W (1983) Synapse elimination in neonatal rat muscle is sensitive to pattern of muscle use. Nature 302:614–616. CrossRef Medline
Tomasi C, Manduchi R (1998) Bilateral filtering for gray and color images. In: Proceedings of the 1998 IEEE International Conference on Computer Vision, pp 839–846. Bombay, India. CrossRef
Van Der Loos H (1976) Barreloids in mouse somatosensory thalamus. Neurosci Lett 2:1–6. CrossRef Medline
Veinante P, Deschênes M (1999) Single- and multi-whisker channels in the ascending projections from the principal trigeminal nucleus in the rat. J Neurosci 19:5085–5095. Medline
Veinante P, Jacquin MF, Deschênes M (2000) Thalamic projections from the whisker-sensitive regions of the spinal trigeminal complex in the rat. J Comp Neurol 420:233–243. CrossRef Medline
Voiculescu O, Charnay P, Schneider-Maunoury S (2000) Expression pattern of a *Krox-20/Cre* knock-in allele in the developing hindbrain, bones, and peripheral nervous system. Genesis 26:123–126. CrossRef Medline
Wang H, Zhang ZW (2008) A critical window for experience-dependent plasticity at whisker sensory relay synapse in the thalamus. J Neurosci 28:13621–13628. CrossRef Medline
Wang H, Liu H, Zhang ZW (2011a) Elimination of redundant synaptic inputs in the absence of synaptic strengthening. J Neurosci 31:16675–16684. CrossRef Medline
Wang H, Liu H, Storm DR, Zhang ZW (2011b) Adenylate cyclase 1 promotes strengthening and experience-dependent plasticity of whisker relay synapses in the thalamus. J Physiol 589:5649–5662. CrossRef Medline
Watson C, Paxinos G (2010) Chemoarchitectonic atlas of the mouse brain. San Diego: Academic.
Williams MN, Zahm DS, Jacquin MF (1994) Differential foci and synaptic organization of the principal and spinal trigeminal projections to the thalamus in the rat. Eur J Neurosci 6:429–453. CrossRef Medline
Wong ROL, Lichtman JW (2003) Synapse elimination. In: Fundamental neuroscience, Ed 2 (Squire LR, Bloom FE, McConnell SK, Roberts JL, Spitzer NC, Zigmond MJ, eds), pp 533–554. San Diego: Academic.
Yamakado M (1985) Postnatal development of barreloid neuropils in the ventrobasal complex of mouse thalamus: a histochemical study for cytochrome oxidase. No To Shinkei 37:497–506. Medline
Zhang ZW, Peterson M, Liu H (2013) Essential role of postsynaptic NMDA receptors in developmental refinement of excitatory synapses. Proc Natl Acad Sci U S A 110:1095–1100. CrossRef Medline